State resolved inelastic scattering of N_2 from Ru(0001)

H. Mortensen,[a] E. Jensen, L. Diekhöner,[b] A. Baurichter, A. C. Luntz, and V. V. Petrunin
Fysisk Institut, University of Southern Denmark, Campusvej 55, DK-5230 Odense M, Denmark

(Received 29 January 2003; accepted 26 March 2003)

Detailed measurements of state resolved inelastic scattering of N_2 from Ru(0001) are reported for a wide range of initial energies (0–3 eV) and angles of incidence. The ion time-of-flight resonantly enhanced multiphoton ionization (REMPI) detection scheme developed here and used with cw molecular beams simultaneously measures the internal quantum state and translational energy normal to the sample surface. Doppler broadening of the REMPI spectrum of scattered particles yields the dispersion in scattering out of plane. The results are qualitatively similar to inelastic N_2 scattering studies for a wide variety of other metal surfaces; i.e., no observable vibrational excitation, weak rotational excitation described as a Boltzmann distribution, strong surface excitation depending upon the incident normal energy, and an anticorrelation between rotational and surface excitation. The absence of any vibrational excitation at $E \approx 3$ eV is inconsistent with adiabatic model dynamics based on the *ab initio* potential-energy surface. It is, however, consistent with a strong nonadiabatic damping of vibration to electron-hole pairs in the region of the barrier. This same suggestion was previously found necessary to rationalize unusual dissociative adsorption and associative desorption of N_2 on Ru(0001). © *2003 American Institute of Physics.*
[DOI: 10.1063/1.1575210]

I. INTRODUCTION

Understanding the kinetics and dynamics of the dissociative adsorption of N_2 on Ru(0001) terraces has been the center of much experimental[1–7] and theoretical[8–10] activity in recent years. In part, this interest derives from the possible importance of supported Ru particles as an end catalyst for NH_3 synthesis, although it has recently been shown that the rate limiting step in NH_3 synthesis is dissociation at steps/defects.[6,11] However, it is also of interest because it is an excellent prototype for direct activated dissociative adsorption, but has a quite different potential-energy surface (PES) topology than the well studied activated adsorptions of H_2 on Cu single crystals[12,13] and CH_4 dissociation on transition-metal surfaces,[14,15] and most of our fundamental concepts and understanding of activated adsorption are based on detailed experimental and theoretical studies on these two. Thus detailed reactive dynamic studies on $N_2/Ru(0001)$ provide a test of the generality of the dynamics lessons learned from the other two systems. Below we summarize a few pertinent aspects of N_2 dissociation dynamics on Ru(0001).

Density-functional calculations (DFT) have shown that the adiabatic barrier to N_2 dissociation on Ru(0001) is $V^* \approx 1.9$ eV and is located along the vibrational coordinate, i.e., it represents a high exit channel barrier.[8–10] These calculations also demonstrate that formation of a π bonded molecularly adsorbed state is endothermic by 0.5 eV so that there are no π bonded molecular precursors in the dissociative adsorption, i.e., it is a direct dissociation. Previous molecular-beam studies of the direct dissociative adsorption of $N_2/Ru(0001)$ have been recently summarized and are quite unusual relative to expectations based on H_2/Cu and CH_4 dissociations.[2] Especially puzzling are that the dissociation probability $S_0 \ll 1$ at normal translational energy $E_n \gg V^*$ and that there seems to be only modest dependence of S_0 on the initial vibrational temperature of the N_2. State resolved associative desorption experiments[7] were especially unsettling based on traditional expectations. There was little vibrational excitation of the nascent N_2, in sharp contrast with anticipated desorption dynamics for a high vibrational barrier. In addition, the energy in all N_2 degrees of freedom accounts for only $\frac{1}{3}$ of V^* and this implies that $\frac{2}{3}$ of the barrier energy is lost to the surface in the desorption process. Adiabatic dynamical models based on the *ab initio* PES from DFT calculations and all known models of how the reaction couples to the lattice were inconsistent with a strong energy loss from the vibrational coordinate to the lattice (phonons).[7] It was shown that the addition of strong nonadiabatic coupling of the vibrational coordinate to electron-hole pairs did resolve the discrepancy and this was taken as *indirect* evidence for the strong nonadiabatic coupling. Inclusion of this nonadiabatic coupling also gave qualitative agreement with the unusal dissociative adsorption behavior. It was also suggested that strong nonadiabatic coupling arose because multiple π bonds are broken/made causing large charge transfer and because the high exit channel (vibrational) nature of the barrier requires strong vibrational excitation.

It has often been argued theoretically that elastic and state resolved inelastic scattering on reactive systems can also be used to probe aspects of the reactive dynamics,[16] especially at incident energies comparable to the dissociation barrier. In that case, significant dissociation is also occurring

[a]Present address: Physics Department, Rutherford Bldg., McGill University, 3600 University St., Montreal, QC, H3A 2T8, Canada.
[b]Present address: Max-Planck-Institut für Festkörperforschung, D-70569 Stuttgart, Germany.

simultaneously with scattering. For example, strong vibrational excitation of H_2 and D_2 scattering from Cu(111) at $E_n \geqslant V^*$ is interpreted in terms of the dissociation barrier topology (at impact sites different from that giving the lowest adiabatic barrier).[13,16] In this paper we report state resolved inelastic scattering experiments for N_2 scattered from Ru(0001) in order to see if any new insight can be gained into the reactive dynamics of this system. The experiments use well defined initial conditions obtained from seeded supersonic nozzle beams and use ion time-of-flight resonantly enhanced multiphoton ionization (REMPI) detection to measure energy partitioning into translation perpendicular to and parallel to the surface, rotation, and vibration. Since all N_2 degrees of freedom are measured, we can also infer the loss to the surface. Since trapping is minimal under the conditions of the experiments,[17,18] the scattering represents direct inelastic scattering. These results are compared to several other studies of the inelastic scattering of N_2 from metals[19–29] and the general energy partitioning for $N_2/\mathrm{Ru}(0001)$ scattering is found to be quite similar to all prior systems studied. Hence there seems little direct signature of the reactive dynamics in the scattering. The same conclusion was previously obtained for the reactive system $N_2/\mathrm{W}(110)$.[24] In comparing the observed lack of vibrational excitation in $N_2/\mathrm{Ru}(0001)$ scattering at high E_n with dynamical models, however, it is suggested that this is more compatible with the nonadiabatic dynamics developed to explain the reactive dynamics rather than adiabatic dynamics.

II. EXPERIMENT

All experiments are performed in a molecular-beam-surface science machine that has been described in detail previously.[30,31] Incident N_2 molecules in the scattering experiments are derived from triply differentially pumped supersonic molecular beams, either neat (for low incident energies) or as a dilute seed in either He or H_2 for higher incident energies. The incident energy, variable from $\sim$0 to 3 eV, is controlled by varying the seed mixture and the nozzle temperature T_n. Translational energy distributions of all incident N_2 beams are measured using conventional chopped beam time-of-flight techniques. Certain low-energy experiments are conducted using a high Mach number stainless steel nozzle with energy resolution $\Delta E/E \approx 0.05$ and low rotational state distributions ($T_{\mathrm{rot}} \sim 20$ K). In order to minimize the possibility of catalytic reaction in a hot nozzle when seeding N_2 in H_2, we use an alumina (Al_2O_3) ceramic nozzle in that case. This nozzle has a larger orifice and lower Mach numbers. Typical energy widths using the ceramic nozzle at high T_n are $\Delta E/E \approx 0.15$, with initial rotational temperatures varying with T_n, but generally $\leqslant$300 K. The beam diameter at the surface is roughly the same as that of the 9-mm diameter Ru(0001) crystal.

Procedures for cleaning, handling, and characterization of the very high quality Ru(0001) single crystal have been described elsewhere.[1] In the experiments reported here, the Ru(0001) crystal is initially cleaned by temperature programmed oxidation followed by 10-s annealing at 1600 K to remove oxygen just prior to beam exposure. Sputter-anneal cycles are applied regularly. Most scattering experiments are conducted at a surface temperature $T_s \geqslant 600$ K in order to minimize contamination buildup on the surface during the sometimes lengthy scattering experiments. At this T_s, CO is not stably adsorbed and hydrogen coverage on the surface from the H_2 seeded beams is $<1\%$.[32] Buildup of N on the surface due to dissociative adsorption of N_2 does not in general pose any problem by virtue of the low sticking coefficient.[2] During extensive recordings of rotational spectra of high-energy beams, however, the sample was flashed to 1000 K every 30 min, which limits the maximum N coverage in all experiments to $<5\%$. Even with such long exposures, all impurities on the Ru(0001) surface, e.g., oxygen, are below Auger detection limits. In addition, there is no carbon buildup on the surface during the course of the experiments as shown by temperature programmed oxidation.

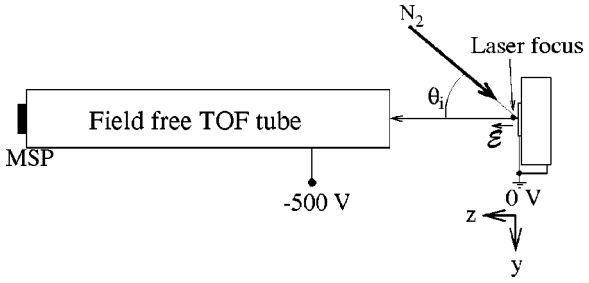

FIG. 1. Sketch of the scattering and REMPI detection system and definition of the coordinate system used throughout the discussion. MSP is the microsphere plate ion detector.

State-resolved detection of the scattered N_2 was obtained by ion time-of-flight resonantly enhanced multiphoton ionization (REMPI) using the (2+1) REMPI scheme first reported by Lykke and Kay.[33] The $\sim$202-nm light required to excite the $a''\,{}^1\Sigma_g^+ \leftarrow X\,{}^1\Sigma_g^+$ transition is produced in a commercial system consisting of a frequency-doubled Nd:YAG pulsed laser (Continuum Powerlite 8010) pumping a tunable dye laser (Continuum ND6000). The output of the dye laser (approximately 607 nm) is tripled in a uv-tracking system (Continuum UVT-3). The resulting 202-nm light consisted of approximately 0.6–1-mJ pulses (5 ns) and with a bandwith [full width at half maximum (FWHM)] of $\sim$0.1 cm^{-1}.

The general layout of the scattering experiment and REMPI detector is shown in Fig. 1. The UV light is focused to an approximately 0.1-mm diameter beam propagating parallel to the surface in the $\hat{x}$ direction and at a distance of typically 1 mm from the surface. The N_2^+ ions formed via REMPI are extracted by an electric field into a field-free time-of-flight (TOF) tube and ultimately detected by a microsphere plate. The N_2^+ ions are separated from other ions formed by nonresonant multiphoton ionization by their rough time of flight (TOF) to the detector which is dependent on their mass/charge ratio. Critical dimensions and typical operating conditions are as follows: extraction voltage of -500 V, distance of surface to TOF tube is 35 mm, TOF tube length is 100 mm and active detection region of microsphere plate is 9 mm diameter. The sample bias [necessary for *e*-beam heating of the Ru(0001)] is switched to ground potential during the ionization and detection period. Both the

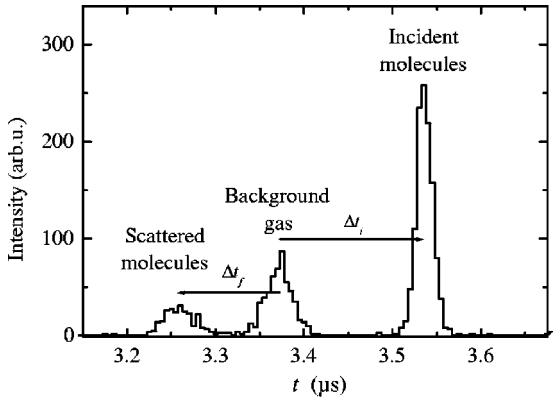

FIG. 2. $N_2(v=0,J=8)$ time-of-flight REMPI spectrum produced by scattering N_2 from Ru(0001) with incidence conditions $E_i=2.7$ eV, $\theta_i=0°$. t is the absolute ion time of flight (TOF). Three classes of N_2 labeled in the figure are identified. Δt_i characterizes the TOF of the incident beam and Δt_f characterizes the TOF of the scattered molecules.

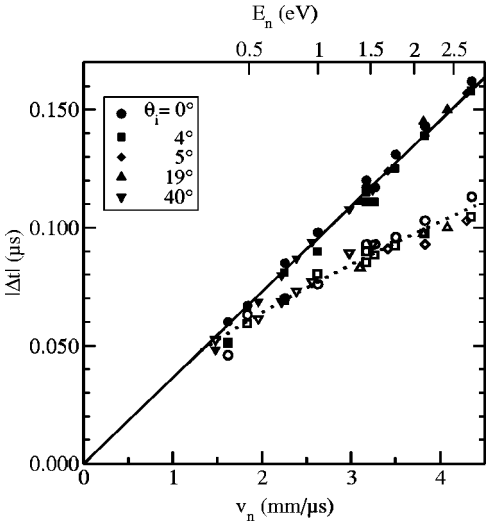

FIG. 3. The absolute value of ion TOF shifts as defined in Fig. 2 as a function of the incident normal velocity v_n (bottom axis) and incident normal energy E_n (top axis) for various incident total energies and angles θ_i as given in legend. $|\Delta t|$ corresponds to $|\Delta t_i|$ for incident N_2 and are the filled symbols. The open symbols are $|\Delta t_f|$ measured for the same incidence conditions as the $|\Delta t_i|$ point vertically above it. The solid line is a linear fit to $|\Delta t_i|$. The dotted line through the points for the scattered molecules is merely drawn to guide the eye.

ion TOF detector and the sample are independently rotatable about the center line of the chamber.

With the N_2 molecular beam incident on the sample, two satellite peaks are observed next to the TOF peak corresponding to rest gas N_2^+ as shown in Fig. 2 for REMPI detection of rotational state $J=8$. This is due to three different velocity groups of the N_2 molecules relative to the extraction field at the point of ionization. These are the incident beam (moving away from the detector), molecules scattered from the surface (moving toward the detector) and background N_2 in the chamber (on average stationary with respect to the detector). The assignment of these three peaks is also confirmed by measuring rotational state distributions for each separately (see discussion later). Thus the ion TOF t is sensitive to velocity and can be used to measure translational energies of N_2 after scattering from the surface.

Generally, velocity measurements of neutrals using ion TOF techniques employ ionization and subsequent drift through a field-free region prior to acceleration by an electric field[34] or ionization at a point in a well defined accelerating uniform electric field.[35] In our REMPI detection scheme (Fig. 1), no special care was taken to generate a uniform electric field between the sample and the entrance to the TOF tube. As a result, the full ion trajectory to the TOF tube is unknown and there is no absolute reference of ion flight times t to velocity. However, near the sample surface the electric field must be uniform and perpendicular to the surface (along $\hat{z}$). The magnitude of Δt, the variation in ion TOF t relative to the background gas with $\langle v\rangle=0$, is dominated by the velocity of N_2 perpendicular to the surface, since the major velocity dependence of t arises when it is near the surface, i.e., before it is accelerated significantly by the electric field. It is shown elsewhere[36] that $\Delta t=-v_n/a+c(v_n)$, where $v_n=\pm\sqrt{2E_n/m}$ is the velocity component normal to the surface and a is the acceleration of the ion at the point of ionization. $c(v_n)$ is a v_n-dependent correction term to account for the fact that the total field from the surface to the entrance of the TOF tube is not uniform. Note that when v_n is directed away from the surface (positive), Δt is negative. Both the constant a and $c(v_n)$ are unknown since the ion trajectory is undoubtedly complex and Δt must be calibrated to v_n with known velocity neutrals. The solid points in Fig. 3 show such a calibration using ion TOF measurements for REMPI of $J=8$ for a N_2 molecular beam with incident energy E_i and incident angle θ_i. Here, E_i was measured accurately by chopped beam TOF techniques using a quadrupole mass spectrometer. As usual, $E_n=E_i\cos^2\theta_i$ and $v_n=v_i\cos\theta_i$. The linearity of the plot of Δt_i versus v_n indicates that the correction term $c(v_n)$ is quite small and can be neglected and the slope of the line gives the constant a. This corresponds to a field strength of approximately 80 V/cm at the point of ionization.

Using this calibration, it is possible to measure the average component of velocity normal to the surface for the scattered molecules $\langle v_f\rangle$ from the shifted peak Δt_f for the scattered component. This is shown in Fig. 3 as the open points. Although the peak positions of the scattered particles were quite reproducible, the broadening in the raw TOF data for the scattered beam relative to the incident beam (see Fig. 2) was not reproducible and therefore must depend on instrumental aspects of the TOF resolution. However, because $\langle v_f\rangle$ is $\gg\Delta v_f$, the dispersion in normal velocity for the scattered molecules, the average normal energy of the scattered N_2 is $\langle E_f\rangle\approx\frac{1}{2}m\langle v_f\rangle^2$. We shall take this to be an equality throughout the discussion. As will be discussed later, considerable energy transfer occurs out of the normal component of translational energy in the scattering, so the absolute magnitudes of the scattered N_2 delays, i.e., $|\Delta t|$, are smaller than those of the incident beam.

Trajectory simulations for limiting cases of the field distribution indicate a very broad angular acceptance for scattering in the ion TOF detector, and whose magnitude depends somewhat on $\langle v_f\rangle$. In most experiments, the angular acceptance is $\geqslant 50°$. The center of the broad angular accep-

tance range depends on alignment of the ion detector relative to the surface (vertically and horizontally). Alignment was achieved by maximizing ion signals of the incident molecular beam. This centers the broad angular acceptance for the condition that conserves parallel momentum in the scattering. As discussed later, changes in parallel velocity as a result of scattering are small enough that most of the scattered particles are detected irrespective of their velocity parallel to the surface.

The velocity distribution parallel to the surface and in the direction of laser propagation ($\hat{x}$) can be estimated by measuring the Doppler broadening of the REMPI resonance for a single rotational transition. Assuming that the velocity distribution parallel to the surface is Maxwellian, e.g., as formed by some angular distribution of scattering, Doppler broadening produces a Gaussian spectral line shape with FWHM $\Delta\nu_D = 2\nu\sqrt{2\ln 2}\Delta v_x/c$, where $\Delta v_x = \sqrt{\langle v_x^2\rangle - \langle v_x\rangle^2}$. The total experimentally observed linewidth $\Delta\nu_{\mathrm{exp}}$ is therefore a convolution of the laser linewidth $\Delta\nu_L$ and the Doppler broadening $\Delta\nu_D$. If $\Delta\nu_L$ can also be described by a Gaussian, the three are simply related by $(\Delta\nu_{\mathrm{exp}})^2 = (\Delta\nu_L)^2 + (\Delta\nu_D)^2$. We have calibrated $\Delta\nu_L$ by measuring the experimental lineshape $\Delta\nu_{\mathrm{exp}}$ of a single rovibronic transition of a 300-K background N_2 sample and correcting for the known Doppler broadening with the relation above. The linewidth of $\Delta\nu_L = 0.13\,\mathrm{cm}^{-1}$ obtained is in good agreement with the laser specifications and was found to be very reproducible and stable during the several months of experiments.

Internal state distributions of initial and scattered N_2 are obtained by integrating the respective REMPI TOF signals over t. The REMPI intensity I_{REMPI} for a given transition is related to the density of the initial internal state $n(v,J)$ by the simple relation $I_{\mathrm{REMPI}} \propto n(v,J) I_{\mathrm{UV}}^2$, where I_{UV} is the UV laser intensity. No corrections for rotational line strengths nor vibrational Franck–Condon factors are necessary for (2+1) REMPI of N_2,[33,37] nor is the (2+1) REMPI intensity very sensitive to any alignment or orientation of N_2 produced by scattering.[37,38] The dependence of I_{REMPI} on I_{UV} was verified experimentally over an order of magnitude change in I_{UV} and presumably infers that the ionization step is strongly saturated for our laser focusing conditions. It was necessary to include the I_{UV} term in the analysis of REMPI intensities since I_{UV} changed by roughly 20% when scanned through the entire spectral range used in the experiments. The ability to obtain relative internal state distributions from REMPI intensities was verified by measuring the rotational and vibrational state distributions for known distributions. For example, background N_2 in the chamber gave a Boltzmann distribution for $n(v=0,J)$ with $T_{\mathrm{rot}} = 316\,\mathrm{K} \pm 16\,\mathrm{K}$. In addition, measurements of $n(v=1):n(v=0)$ for a hot nozzle molecular beam agreed well with measurements of the nozzle temperature T_n. Although densities are measured, fluxes are the appropriate quantity to compare with theoretical interpretations of the scattering. However, since $\Delta t \propto \sqrt{E_n}$, the flux $F(v,J,E) \propto n(v,J,\Delta t)$ so that no Jacobian corrections derive from the flux-density transformation.

III. EXPERIMENTAL RESULTS AND DISCUSSION

The presentation and qualitative discussion of the results is first divided into four sections according to the various N_2 degrees of freedom probed in the scattering; vibrational, rotational, translational energy parallel to the surface, and translational energy perpendicular to the surface. When combined, these measurements give the total energy lost to the surface in the scattering process as described in a fifth section. A sixth section deals with correlations between the different scattering channels. In all cases, initial states for the scattering were produced by (seeded) supersonic nozzle beams of N_2 and the full initial distributions (v,J,E_i,θ_i) were well characterized.

A. Vibrational excitation

Low rotational states in the $v=1 \leftarrow v=1$ vibrational band are readily detected using (2+1) REMPI.[33] Higher rotational states ($J>13$) apparently suffer perturbations so their assignment and intensities are subject to some uncertainty.[37] Thus, by comparing relative intensities of low J transitions of $v=1$ to those of $v=0$ before and after scattering, we obtain the extent of vibrational excitation produced in the scattering. This assumes that the rotational state distributions are the same in the two vibrational states. Although we cannot verify this experimentally, there is no reason to suspect this is not approximately true. At low incident normal energy $E_n \approx 1$ eV, no vibrational excitation is observed in the scattering, $\langle \Delta E_v \rangle \approx 0$. Even at high incident energy, $E_n \approx 2.8$ eV, no measurable vibrational excitation is observed. In this case, however, because of the high rotational excitation produced in the scattering (see next section), there is overlap of transitions of $v=0$, $J>49$ with the low J transitions of $v=1$. As a result, we can only determine an upper bound to $v=1$ excitation. In addition, no measurable excitation for $v>1$ was observed. We thus find that the amount of vibrational excitation created via scattering $\langle \Delta E_v \rangle \leqslant 0.05$ eV at $E_n \approx 2.8$ eV.

Vibrational excitation and de-excitation has previously been observed as significant for H_2 and D_2 scattered from Cu(111) (Refs. 39 and 40) at E_n comparable to the adiabatic barrier height for dissociation. This has been rationalized as due to a strong coupling between the normal translational and vibrational coordinates caused by a softening of the H–H stretch in the neighborhood of the barrier,[16,41,42] i.e., as a consequence of the ''exit'' channel or vibrational nature of barrier. The two-dimensional potential-energy surface (PES) for N_2 dissociation on Ru(0001) obtained in DFT calculations[10] exhibits a barrier of $\sim$2 eV almost exclusively along the vibrational coordinate. Thus we anticipate that there should be significant N_2 vibrational excitation in scattering at $E_n \geqslant 2$ eV by the same mechanism operative for H_2/Cu. Adiabatic model dynamics calculations described in Sec. V confirm this anticipation. In that section, we also suggest that nonadiabatic coupling to electron-hole pairs may be responsible for the absence of observable vibrational excitation in the experiments.

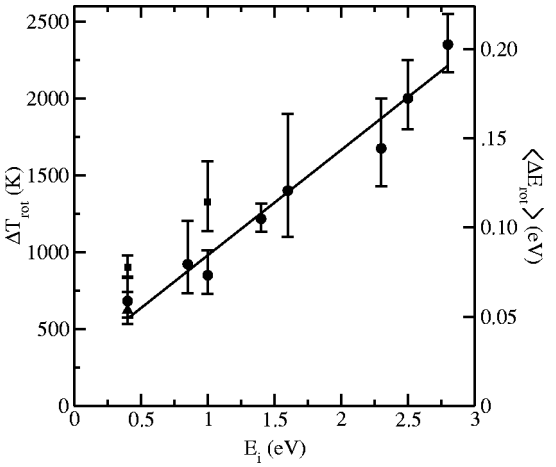

FIG. 4. The increase in rotational temperature ΔT_{rot} (left axis) and the corresponding average rotational energy $\langle \Delta E_{\mathrm{rot}} \rangle$ (right axis) as a function of total incident translational energy E_i. The circles correspond to experiments at a surface temperature $T_s = 610$ K, the squares at $T_s = 1000$ K and the triangle at $T_s = 300$ K. The line is a linear fit to ΔT_{rot} at $T_s = 610$ K.

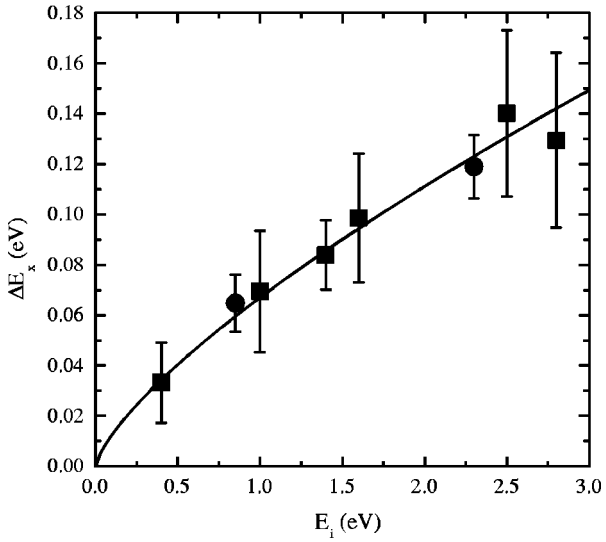

FIG. 5. Doppler measurements of the conversion of incident energy E_i into translational energy parallel to the laser propagation direction ΔE_x. The squares correspond to $\theta_i = 19°$ and circles to $\theta_i = 40°$. The line through the data is simply to guide the eye and has no theoretical significance.

B. Rotational excitation

Extensive rotational excitation of diatomic molecules scattered from surfaces is a very well-known phenomenon; sometimes exhibiting rotational rainbows[43] and sometimes simply producing rotationally hot Boltzmann distributions.[23,24,29] For N_2 scattering from Ru(0001), only Boltzmann rotational distributions are observed for all incident E_i and θ_i. Incident beams are also well characterized by (much lower) Boltzmann rotational distributions whose rotational temperature depends on nozzle temperature T_n and expansion characteristics. To account for the varying initial rotational content of the beams for different initial conditions, we characterize the rotational excitation by the increase in rotational temperature in the scattering experiment ΔT_{rot}. The average rotational energy created in the scattering is $\langle \Delta E_{\mathrm{rot}} \rangle = k_B \Delta T_{\mathrm{rot}}$. In Fig. 4, we plot ΔT_{rot} and the equivalent average rotational energy versus E_i. The error bars given in the figure correspond to twice the standard deviations of Boltzmann fits to the rotational populations. Experiments presented in Fig. 4 are at $\theta_i = 4°$, 20°, and 40° and show that ΔT_{rot} scales approximately with E_i rather than E_n. The dependence of ΔT_{rot} on E_i is seen to be approximately linear at $T_s = 610$ K with an offset in the extrapolation to $E_i = 0$. A very few spectra were recorded with different T_s as indicated in the figure. ΔT_{rot} increases slightly with T_s as well.

In early studies of rotational excitation, it was shown that the average rotational excitation can be approximately described by a bilinear expression[43,44]

$$\langle \Delta E_{\mathrm{rot}} \rangle = a(E_i + \langle E_w \rangle) + b k_B T_s, \tag{1}$$

where a, b, and $\langle E_w \rangle$ are constants. Neglecting the T_s dependent term (i.e., assuming $b = 0$) and fitting the results at $T_s = 610$ K, we find $a = 0.06$ and $\langle E_w \rangle = 0.43$ eV. $\langle E_w \rangle$ has often been interpreted as the molecule-surface well depth,[43,44] although there is only empirical justification for this. We do note that the experimental binding energy for $N_2/\mathrm{Ru}(0001)$ is 0.44 eV at $\Theta_N = 0.33$,[45] in (too) good agreement with this empirical assignment. The limited measurements of the T_s dependence would imply $b \approx 0.4$–0.7, although there are insufficient measurements of the T_s dependence to actually ascertain whether Eq. (1) represents this dependence well.

C. Excitation of translation parallel to the surface

Due to corrugation, either thermally induced or static, scattering can change the momentum and energy parallel to the surface $E_\parallel$. This is often described by measuring the angular distributions in and out of the scattering plane, i.e., along the $\hat{y}$ and $\hat{x}$ directions, respectively. As described previously, the dispersion in the velocity distribution out of the scattering plane along the direction of laser propagation Δv_x can be measured by the Doppler broadening of spectral lines. Since undoubtedly $\langle v_x \rangle = 0$ out of the scattering plane, the scattering along this direction can be described by the dispersion in the translational energy $\Delta E_x = \frac{1}{2} m \langle v_x^2 \rangle = \frac{1}{2} m (\Delta v_x)^2$. In Fig. 5, measurements of ΔE_x obtained from the Doppler broadening are shown as a function of the total incident energy E_i. For each (E_i, θ_i) the widths of several rotational lines around $J = 16$ were averaged. The smooth line through the points is drawn only as a visual guide. Similar to rotational excitation, ΔE_x scales approximately with E_i rather than E_n. The increase in ΔE_x with E_i is consistent with a well-known increase in corrugation with E_i. However, relative conversion along $\hat{x}$, $\Delta E_x / E_i$, decreases from ~ 0.08 to 0.05 as E_i increases.

For normal incidence, the conversion of incident translational energy into both x and y motion parallel to the surface must be identical by symmetry. In this case $\langle v_x \rangle = \langle v_y \rangle = 0$, and reasonably assuming that scattering into the two degrees of freedom are uncoupled, implies that conversion of E_i into translational energy parallel to the surface is defined by the root-mean-square energy transfer $\Delta E_\parallel = 2 \Delta E_x$. For $\theta_i \neq 0$, there is no rigorous relation between ΔE_y and ΔE_x. However, since the scattering peaks at or near the specular condition,[46] it is still likely that ΔE_y

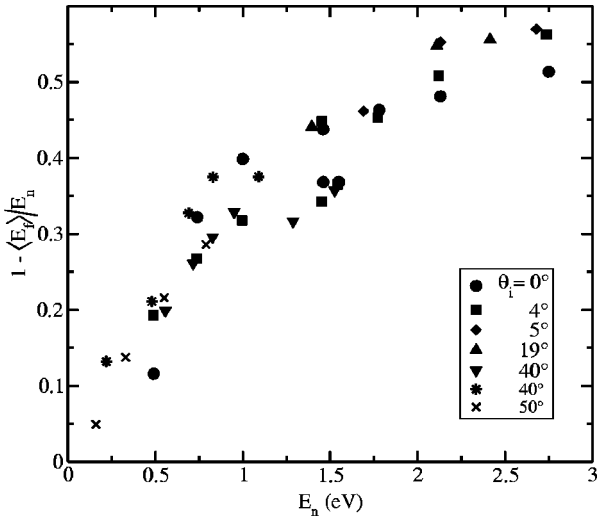

FIG. 6. The average fractional normal translational energy loss in scattering, $1-\langle E_f\rangle/E_n$, as a function of incident normal energy E_n for rotationally elastic scattering. The filled points are state resolved measurements for the $v=0$, $J=8$ rovibrational state and with a surface temperature $T_s=610$ K. The stars and crosses are extracted from the results of Ref. 46 (see text). Angles of incidence θ_i are given in the legend.

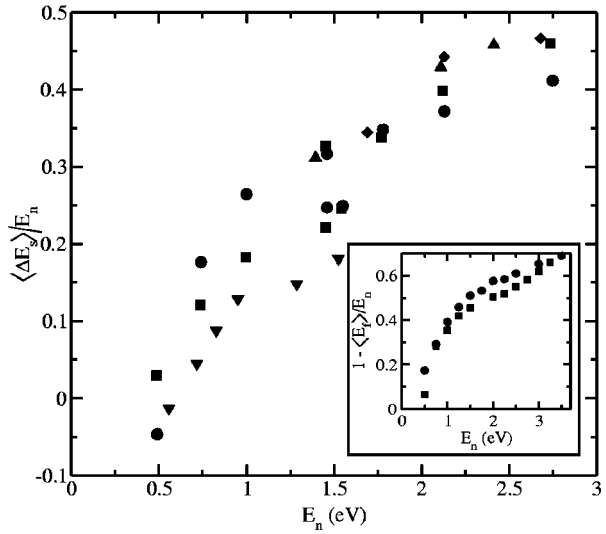

FIG. 7. The average fractional energy loss to the surface $\langle\Delta E_s\rangle/E_n$ for normal incidence conditions and rotationally elastic scattering as a function of E_n. Points were obtained by combining the results in Figs. 6 and 5. The inset shows the predicted translational energy loss $1-\langle E_f\rangle/E_n$ from the adiabatic (circles) and nonadiabatic (squares) dynamical models.

$\approx\Delta E_x$ and that $\Delta E_\parallel\approx 2\Delta E_x$. From Fig. 5, at the highest near normal energy corresponding to $E_i=2.8$ eV, $\Delta E_\parallel\approx 0.25$ eV, i.e., the excitation of translational energy parallel to the surface is modest.

We obtain an estimate of the angular distribution out of the scattering plane (FWHM $\Delta\theta_x$) as $\tan(\Delta\theta_x/2)=\sqrt{2\ln 2}\Delta v_x/\langle v_f\rangle$. This gives approximately $\Delta\theta_x\approx 35-45°$ for the various incidence conditions. This is somewhat larger than the angular widths of $\Delta\theta_y\approx 15-25°$ observed in the scattering plane by conventional molecular-beam scattering at $\theta_i=40°$.[46] Note, however, that $\Delta E_y\approx\Delta E_x$ implies that $\Delta\theta_y<\Delta\theta_x$ at high θ_i.

D. Normal translational energy loss

As explained previously, the TOF delays of the incident beam relative to the background gas give a calibration of Δt in terms of velocity or translational energy normal to the surface. Thus by comparing $|\Delta t|$ for scattered N_2 relative to this calibration, we can measure the average normal translational energy $\langle E_f\rangle$ of the scattered N_2. The open points in Fig. 3 are the $|\Delta t_f|$ values for scattered N_2. The $|\Delta t_i|$ measured for the corresponding incident beams are determined by E_n and are given as the solid points above each open point. The decrease in $|\Delta t|$ for each initial condition (E_i,θ_i) is due to energy loss from the normal component of translational energy upon scattering. This is best represented as the fractional normal energy loss upon scattering, $1-\langle E_f\rangle/E_n=1-(\Delta t_f/\Delta t_i)^2$. Values of this quantity obtained from the data of Fig. 3 are plotted in Fig. 6 versus E_n as the solid points. The fractional normal energy loss scales approximately with E_n rather than E_i and increases with increasing incident energy, from ~10% at $E_n\approx 0.5$ eV to approximately 50% at $E_n\approx 2.7$ eV. All points in this plot refer only to REMPI detection of the $J=8$ rotational state and represent essentially rotationally elastic scattering.

Using conventional chopped molecular-beam and TOF detection with a mass spectrometer detector, Papageorgopoulos *et al.*[46] have previously measured the translational energy and angular distributions for N_2 scattering from Ru(0001). Since their measurements integrate over all quantum states but are angularly resolved, while our results are quantum state resolved but only measure the average energy along the normal and parallel to the surface, the two experiments are not directly comparable. However, by considering only the normal component in the specularly scattered results of Papageorgopoulos *et al.*, and correcting their results for rotational excitation as observed by us, we can approximately transform their results to a form equivalent to ours for rotationally elastic scattering. These are given by asterisks (*) and crosses (x) in Fig. 6 for $\theta_i=40°$ and 50°, respectively. There is very good agreement of our data with those measured by Papageorgopoulos *et al.* This justifies the calibration procedures used in the analysis of the ion TOF REMPI measurements of energy loss.

E. Surface excitation

Energy loss from normal translation must occur by vibrational excitation ΔE_v, rotational excitation $\Delta E_{\rm rot}$, conversion to parallel translational motion $\Delta E_\parallel$, or loss to the surface (phonon or electronic excitations) ΔE_s. It was shown in the previous sections that $\langle\Delta E_v\rangle$, $\langle\Delta E_{\rm rot}\rangle$, and $\Delta E_\parallel$ are all modest, so that the normal energy loss must be dominated by loss to the surface at high incident energies. Combining all energy measurements for the rotationally elastic measurements $(J=8)$ of Fig. 6 and estimates of $\Delta E_\parallel\approx 2\Delta E_x$ from Fig. 5, we obtain the average energy lost to the surface $\langle\Delta E_s\rangle=E_n-\langle E_f\rangle-\Delta E_\parallel-\langle\Delta E_v\rangle$. The fractional loss to the surface in scattering $\langle\Delta E_s\rangle/E_n$ is shown in Fig. 7 as a function of E_n. The approximate scaling of the energy loss to the surface with E_n rather than E_i is consistent with a

TABLE I. The partitioning of energy loss at low, intermediate, and high energies for rotational state $J=8$ upon normal incidence. All energies are given in eV.

E_n	0.50	1.0	2.8
$\langle E_f \rangle$	0.4	0.65	1.3
$\Delta E_{\parallel}$	0.08	0.13	0.3
$\langle \Delta E_s \rangle$	0.02	0.22	1.2

surface energy loss to both phonons[47] and electron-hole pairs.[48] It is certainly anticipated that the heavy N_2 should readily excite phonons on impact[47] so that this must represent a major if not dominant surface loss channel in scattering. The increase in fractional energy loss in Fig. 7 with E_n is well documented for a quite wide range of E_n in other systems.[49] In Sec. V, we compare the results of Fig. 7 with model dynamics calculations for both energy loss to phonons and to electronic excitations of the surface.

Table I summarizes the partitioning of E_n in N_2 scattering for a few representative E_n (assuming normal incidence and rotationally elastic scattering). At low E_n, loss of E_n is dominated by conversion to parallel momentum via the static corrugation as well as the thermally induced roughness of the surface, while the energy loss to the surface is minimal. This is consistent with the broad angular distributions seen at low E_n in molecular-beam scattering.[46] On the other hand, at high E_n, the normal energy loss is dominated by loss to the surface since this increases much more rapidly than the corrugation with E_n.

F. Correlations between energy-transfer channels

Some of the different channels for energy transfer are coupled. Thus the partitioning of energy into one channel depends not only on the incident energy, but also on the other channels detected simultaneously. Here we discuss the couplings observed between energy transfer to the lattice, rotational excitation, and parallel translational motion.

By measuring Δt_f for various rotational states at fixed incident conditions (E_i, θ_i), we measure the coupling between rotational excitation and translational energy loss (principally to the surface). Results for such measurements are shown in Fig. 8(a) for three different E_i. The filled symbols show the dependence of the final normal translational energy E_f on the state resolved rotational energy $E_{\rm rot}$ (bottom axis) or rotational state J (top axis) detected. Figure 8(b) shows the same results, but replotted as $\langle \Delta E_s \rangle / E_n = 1 - (\langle E_f \rangle + \Delta E_{\parallel} + \langle \Delta E_{\rm rot} \rangle + \langle \Delta E_v \rangle)/E_n$ versus $E_{\rm rot}$. This demonstrates the well-known anticorrelation between rotational excitation and surface excitation.[19,50] The slope of this anticorrelation is $d\Delta E_s / dE_{\rm rot} \approx -0.5$. Many different explanations have been suggested for this anticorrelation,[19,24,47,50] although the generality of the phenomenon makes each specific explanation for a given system somewhat suspect.

Finally, by comparing the Doppler broadening of several rotational states $J=16$ to 44 for $E_n = 2.7$ eV, we observe no or at best a very small variation in ΔE_x with increasing $E_{\rm rot}$. Because this correlation was so weak, it was neglected in determining the rotation surface loss anticorrelation $d\Delta E_s / dE_{\rm rot}$ discussed above.

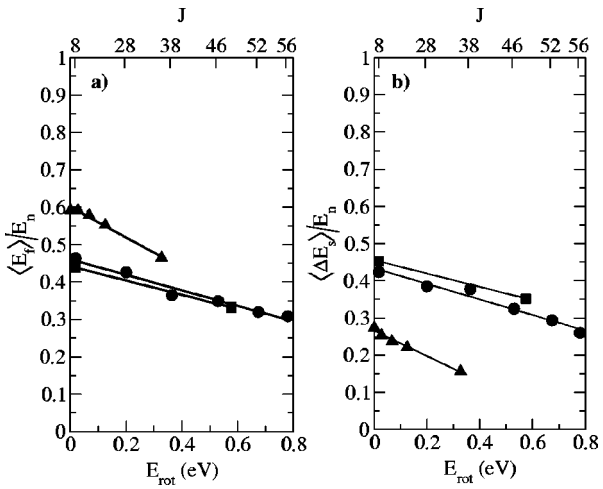

FIG. 8. (a) The average fractional conservation of normal translational energy $\langle E_f \rangle / E_n$ as a function of rotational energy $E_{\rm rot}$ (bottom axis) or rotational quantum number J (top axis). Initial conditions of the experiments are $E_i = 1.5$ eV, $\theta_i = 19°$ (triangles), $E_i = 2.4$ eV, $\theta_i = 0°$ (circles), and $E_i = 2.7$ eV, $\theta_i = 19°$ (squares). (b) Average fractional energy loss to the surface $\langle \Delta E_s \rangle / E_n$ as a function of rotational energy $E_{\rm rot}$ Incidence conditions and symbols are the same as in (a).

IV. COMPARISON TO OTHER N_2/METAL STUDIES

There have been many previous state resolved studies of N_2 scattering from metal surfaces: Ag(111),[19–22] W(110) and Pt(111),[23,24] Pd(111),[25] Au(111),[26] Cu(110),[27,28] and Ni(111).[29] The initial scattering conditions of the experiments vary considerably as well as the completeness of the studies. However, in all cases initial translational energy is partitioned with a large loss to the lattice (20–60% depending upon E_n), a small loss to rotation (<10%) and negligible loss to molecular vibration. The scattering of N_2/Ru(0001) observed here is in complete accord with these general tendencies. Even the parameters extracted to describe the energy transfer are similar for all systems. For example, the value of $a \approx 0.06$ obtained here for N_2/Ru(0001) in Eq. (1) describing average rotational excitation is quite similar to that of several other systems; e.g., 0.07 for N_2/Cu(110),[27] 0.09 for N_2/W(110),[24] while the (uncertain) estimate of $b \approx 0.4$–0.7 obtained here is somewhat larger than the values of 0.1–0.3 measured for N_2/Cu(110).[27] Even the slope of the anticorrelation $d\Delta E_s / dE_{\rm rot} \approx -0.5$ is similar to that observed in many other systems, e.g., -0.6 for N_2/Cu(110),[27] -0.57 for N_2/W(110),[24] and -0.3 for N_2/Ag(111).[19] Finally, the magnitude of the fractional energy loss to the surface given in Fig. 7 is quite comparable to that of other systems at equivalent E_n, e.g., 0.3 at $E_n = 0.79$ eV for N_2/Cu(110),[27] 0.38 at $E_n = 0.75$ eV for N_2/W(110),[24] and 0.4 at $E_n = 0.75$ eV for N_2/Ag(111).[51]

Although the overall energy partitioning is rather similar for all N_2/metal systems, the detailed behavior, e.g., of rotational distributions, differs markedly. However, all systems seem to belong to one of two general qualitative classes of behavior. In one, the scattering is characterized by

rotational rainbows with $\langle \Delta E_{\mathrm{rot}} \rangle$ scaling with E_n and exhibiting strong rotational alignment and orientation. Examples of this behavior include $N_2/Ag(111)$,[19–22] $N_2/Au(111)$,[26] and $N_2/Cu(110)$,[27] as well as the prototype system NO/Ag(111).[43,52,53] In the other class, the scattering gives essentially Boltzmann rotational distributions, $\langle \Delta E_{\mathrm{rot}} \rangle$ scales with E_i rather than E_n, and the rotational alignment/orientation is minimal. This class includes $N_2/W(110)$,[23,24] $N_2/Pt(111)$,[24] $N_2/Pd(111)$,[25] and $N_2/Ni(111)$.[29] Clearly our results for $N_2/Ru(0001)$ are similar to those of this latter class.

The exact nature of the difference in the two classes is unclear. The first class is consistent qualitatively with a purely repulsive interaction of the molecule with the surface, e.g., as an ellipsoid scattering from a smooth surface cube. The interaction responsible for the second class is not yet well understood. It has been suggested previously that the behavior of the second class is due to corrugation,[20–22,51] reactive interactions,[24] or multibounce scattering trajectories.[27,28] However, only $N_2/W(110)$ is dissociative so that the difference seems unrelated to the reactivity of the surface. Nor are N_2 chemisorption well depths markedly different for the two classes so that there is no reason to suspect wide variations in corrugation in the molecular potentials, either in the attractive well or repulsive wall. One possible difference between the two classes is the absence or presence of metal *d* bonding in the N_2 chemisorption interaction, as well as the absence or presence of only partially occupied metal *d*-band states. How either may affect the rotational scattering, however, is at this stage merely speculation. It is possible that *d*-bonding contributions make some corrugation not evident by simply considering the well depths as a measure of chemical interaction. It is also possible that electronic excitations to empty *d*-band states near the Fermi energy could affect the inelastic scattering behavior in some way.

V. MODEL DYNAMICS

We have recently presented a three-dimensional (3D) quasiclassical dynamical model of dissociative adsorption and associative desorption of $N_2/Ru(0001)$ and compared this with detailed experiments.[7] The three dimensions included were the translational coordinate *z*, vibrational coordinate *d*, and a single surface phonon coordinate *q*. The 3D interaction potential was based on the two-dimensional (2D) *ab initio* potential-energy surface obtained in DFT calculations and coupling to the lattice via "dynamic recoil." Translational energy and vibrationally resolved dissociation probabilities $S(E,v,T_s)$ and associative desorption fluxes $D_f(E,v,T_s)$ were calculated in the model by averaging many quasiclassical trajectories over appropriate initial conditions and compared with experiments. It was concluded there that there were qualitative discrepancies between this adiabatic model and the experiments. It was especially noted that this 3D adiabatic model of the dynamics predicted very strong vibrational excitation (vibrational inversion) in $D_f(E,v,T_s)$, although only modest vibrational excitation was observed experimentally. It was also pointed out that only $\frac{1}{3}$ of the energy of the barrier ended up in any N_2 degree of freedom so that there was massive loss to the surface during associative desorption. It was argued that this was unlikely to be due to the limited dimensionality of the model or more complicated coupling to the phonons and it was suggested that this was indirect evidence for strong nonadiabatic coupling of the vibrational coordinate to electron-hole pairs in the metal. Including such couplings in the 3D model as a vibrational friction (and a fluctuating force to enforce thermal equilibrium of the surface) produced good agreement with all experiments, both in sticking and in associative desorption. However, the vibrational friction needed to be quite large relative to conventional wisdom. Arguments were presented to suggest that vibrational frictions are generally quite large in the neighborhood of the transition state for activated dissociations of π bonded molecules, but the proof of these suggestions must await reliable *ab initio* calculations of the nonadiabatic coupling.

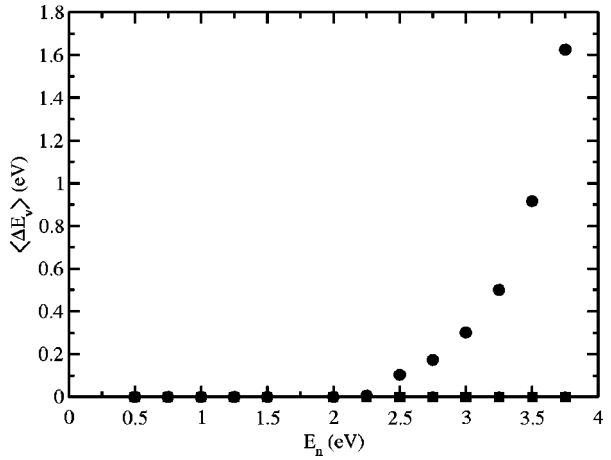

FIG. 9. Average vibrational excitation $\langle \Delta E_v \rangle$ as a function of E_n from the adiabatic (circles) and nonadiabatic (squares) dynamical models.

The same adiabatic and nonadiabatic models can be used to look at inelastic scattering by simply analyzing the nonreactive trajectories. Because the model is 3D, only translation normal to the surface, vibration, and the surface oscillator are defined. Therefore we cannot investigate rotational excitation nor excitation of $E_{\parallel}$ in scattering. We can, however, calculate the average vibrational excitation $\langle \Delta E_v \rangle$, the average phonon excitation $\langle \Delta E_q \rangle$, and the fractional translational energy loss $1-\langle E_f \rangle / E_n$ in both the adiabatic and nonadiabatic models.

$\langle \Delta E_v \rangle$ predicted by the adiabatic and nonadiabatic models are presented in Fig. 9. The adiabatic model predicts a strong increase in vibrational excitation starting at $E_n \approx V^*$. This is similar to the vibrational excitation observed in $D_2/Cu(111)$ scattering.[40] On the other hand, the model with nonadiabatic vibrational coupling shows no evidence of vibrational excitation in scattering. Since the experiment also shows no evidence of vibrational excitation, we take this experimental observation as more consistent with nonadiabatic dynamics. This statement cannot be made too definitively, however, because of experimental uncertainties in establishing the lower limit of vibrational excitation and because of the limited dimensionality of the model. Also, limiting the dynamics to three dimensions seems less appro-

priate for inelastic scattering than for reactive events since scattering undoubtedly arises from $N_2/Ru(0001)$ collisions with all possible orientations and impact parameters. On the other hand, reactive dynamics arises principally from steric sampling of the lowest potential barriers and we believe this is well represented in the 3D model.

$1-\langle E_f\rangle/E_n$ from the models is shown as the inset in Fig. 7. There is no marked difference between the adiabatic and nonadiabatic models. Since $\langle \Delta E_v\rangle = 0$ for the nonadiabatic model, $\langle \Delta E_s\rangle/E_n = 1-\langle E_f\rangle/E_n$ in this case. $\langle \Delta E_q\rangle$ is nearly identical for both models and $\langle \Delta E_v\rangle$ that occurs in the adiabatic model is lost to electron-hole pairs in the nonadiabatic model, so that the total energy lost from translation is nearly identical in the two cases. Excitation of the lattice (phonons) and excitation of vibration (or damping into electron-hole pairs) appear to be nearly independent processes. Presumably, lattice excitation occurs on first impact in the entrance channel, while vibrational excitation/damping occurs only subsequently when the N_2 approaches the barrier. The energy loss in the models is in reasonable agreement with the experiments, both in magnitude and shape.

VI. CONCLUSION

In this paper, we present detailed studies of the inelastic scattering of N_2 from Ru(0001) over a wide range of incident conditions (E_i, θ_i) produced by supersonic molecular beams. State resolved detection of N_2 before and after scattering was accomplished using ion TOF REMPI detection. Our implementation measures the translational energy normal to the surface by the ion TOF and the translational energy parallel to the surface from the Doppler broadening of the REMPI spectra. We observe little or no vibrational excitation of N_2 for incident energies up to 2.8 eV. Rotational excitation is well described by a Boltzmann distribution, which increases linearly with E_i rather than E_n. The overall conversion of translational to rotational energy is less than 10% of E_i, even at $E_i = 2.8$ eV. Measurements of the Doppler broadening of individual rotational transitions allow a measurement of the modest excitation of translational energy parallel to the surface $\Delta E_\parallel$. This also increases somewhat with E_i, but with $\Delta E_\parallel/E_i$ decreasing with E_i. Measurements of the total energy loss out of the normal component of translational energy show that this scales approximately with E_n and increases from $\sim$10% at low E_n to $>$50% at high E_n. Combining all measurements, we obtain the average fractional energy loss to the surface in scattering $\langle \Delta E_s\rangle/E_n$. This increases from $\sim$0 at low E_n to approximately 50% at high E_n. $\langle \Delta E_s\rangle/E_n$ and the rotational energy $E_{\rm rot}$ are anticorrelated and there is at best only a very weak correlation between $\Delta E_\parallel/E_i$ and $E_{\rm rot}$. All experimental results for $N_2/Ru(0001)$ scattering are qualitatively similar to those of other state resolved studies of N_2 scattering from *d*-band transition metals, whether reactive [W(110) (Refs. 23 and 24)] or nonreactive [Pt(111),[24] Pd(111),[25] Ni(111) (Ref. 29)]. We believe that, in the inelastic scattering, the only signature of the dissociative dynamics is the absence of strong vibrational excitation in scattering at high E_i. This is not consistent with adiabatic dynamics based on the 2D DFT PES and models of lattice coupling. We suggest that this is a signature of vibrational damping caused by nonadiabatic coupling of the vibrational coordinate to electron-hole pairs. The same nonadiabatic dynamical model (and vibrational friction) used to rationalize the unusual reactive dynamics, successfully accounts for the lack of vibrational excitation.

ACKNOWLEDGMENTS

The authors gratefully acknowledge partial support of this work by the Danish Research Council under Grants No. 9601724 and No. 51000269. Two of the authors (H.M. and L.D.) thank the Danish Research Academy for support during their Ph.D. studies. We also thank C. T. Rettner and D. J. Auerbach for useful discussion.

[1] L. Diekhöner, A. Baurichter, H. Mortensen, and A. C. Luntz, J. Chem. Phys. **112**, 2507 (2000).
[2] L. Diekhöner, H. Mortensen, A. Baurichter, E. Jensen, V. V. Petrunin, and A. C. Luntz, J. Chem. Phys. **115**, 9028 (2001).
[3] L. Diekhöner, H. Mortensen, A. Baurichter, and A. C. Luntz, J. Chem. Phys. **115**, 3356 (2001).
[4] K. Jacobi, Phys. Status Solidi A **177**, 37 (2000).
[5] R. C. Egeberg, J. H. Larsen, and I. Chorkendorff, Phys. Chem. Chem. Phys. **3**, 2007 (2001).
[6] S. Dahl, E. Törnqvist, and I. Chorkendorff, J. Catal. **192**, 381 (2000).
[7] L. Diekhöner, L. Hornekær, A. Baurichter, V. V. Petrunin, E. Jensen, H. Mortensen, and A. C. Luntz, J. Chem. Phys. **117**, 5018 (2002).
[8] J. J. Mortensen, B. Hammer, and J. K. Nørskov, Phys. Rev. Lett. **80**, 4333 (1998).
[9] B. Hammer, Phys. Rev. B **63**, 205423 (2001).
[10] M. J. Murphy, J. F. Skelly, A. Hodgson, and B. Hammer, J. Chem. Phys. **110**, 6954 (1999).
[11] S. Dahl, R. C. Egeberg, J. H. Larsen, I. Chorkendorff, E. Törnqvist, and J. K. Nørskov, Phys. Rev. Lett. **83**, 1814 (1999).
[12] H. A. Michelsen and D. J. Auerbach, J. Chem. Phys. **94**, 7502 (1991).
[13] G. J. Kroes, Prog. Surf. Sci. **60**, 1 (1999).
[14] A. C. Luntz and J. Harris, Surf. Sci. **258**, 397 (1991).
[15] H. Mortensen, L. Diekhöner, A. Baurichter, and A. C. Luntz, J. Chem. Phys. **116**, 5781 (2002).
[16] G. R. Darling and S. Holloway, Rep. Prog. Phys. **58**, 1595 (1995).
[17] D. C. Seets, M. C. Wheeler, and C. B. Mullins, J. Vac. Sci. Technol. A **14**, 1566 (1996).
[18] D. C. Seets, M. C. Wheeler, and C. B. Mullins, Chem. Phys. Lett. **257**, 280 (1996).
[19] G. O. Sitz, A. C. Kummel, and R. N. Zare, J. Chem. Phys. **89**, 2558 (1988).
[20] G. O. Sitz, A. C. Kummel, R. N. Zare, and J. C. Tully, J. Chem. Phys. **89**, 2572 (1988).
[21] A. C. Kummel, G. O. Sitz, R. N. Zare, and J. C. Tully, J. Chem. Phys. **89**, 6947 (1988).
[22] A. C. Kummel, G. O. Sitz, R. N. Zare, and J. C. Tully, J. Chem. Phys. **91**, 5793 (1989).
[23] T. F. Hanisco and A. C. Kummel, J. Vac. Sci. Technol. A **11**, 1907 (1993).
[24] T. F. Hanisco and A. C. Kummel, J. Chem. Phys. **99**, 7076 (1993).
[25] K. R. Lykke and B. D. Kay, J. Chem. Phys. **90**, 7602 (1989).
[26] K. R. Lykke and B. D. Kay, J. Phys.: Condens. Matter **3**, S65 (1991).
[27] J. L. W. Siders and G. O. Sitz, J. Chem. Phys. **101**, 6264 (1994).
[28] J. L. W. Siders and G. O. Sitz, J. Vac. Sci. Technol. A **13**, 1400 (1995).
[29] C. M. Matthews, F. Balzer, A. J. Hallock, M. D. Ellison, and R. N. Zare, Surf. Sci. **460**, 12 (2000).
[30] A. C. Luntz, M. D. Williams, and D. S. Bethune, J. Chem. Phys. **89**, 4381 (1988).
[31] H. Mortensen, L. Diekhöner, A. Baurichter, E. Jensen, and A. C. Luntz, J. Chem. Phys. **113**, 6882 (2000).
[32] P. Feulner and D. Menzel, Surf. Sci. **154**, 465 (1985).
[33] K. R. Lykke and B. D. Kay, J. Chem. Phys. **95**, 2252 (1991).
[34] H. A. Michelsen, C. T. Rettner, D. J. Auerbach, and R. N. Zare, J. Chem. Phys. **98**, 8294 (1993).
[35] A. Hodgson, Prog. Surf. Sci. **63**, 1 (2000).
[36] E. Jensen, Master's thesis, University of Southern Denmark, 2001.
[37] T. F. Hanisco and A. C. Kummel, J. Phys. Chem. **95**, 8565 (1991).

[38] T. F. Hanisco, C. Yan, and A. C. Kummel, J. Phys. Chem. **96**, 2982 (1992).
[39] C. T. Rettner, D. J. Auerbach, and H. A. Michelsen, Phys. Rev. Lett. **68**, 2547 (1992).
[40] A. Hodgson, J. Moryl, P. Traversaro, and H. Zhao, Nature (London) **356**, 501 (1992).
[41] D. Halstead and S. Holloway, J. Chem. Phys. **93**, 2859 (1990).
[42] G. R. Darling and S. Holloway, J. Chem. Phys. **97**, 734 (1992).
[43] A. W. Kleyn, A. C. Luntz, and D. J. Auerbach, Phys. Rev. Lett. **47**, 1169 (1981).
[44] G. D. Kubiak, J. J. E. Hurst, H. G. Rennagel, G. M. McClelland, and R. N. Zare, J. Chem. Phys. **79**, 5163 (1983).
[45] D. Menzel, H. Pfnür, and P. Feulner, Surf. Sci. **126**, 374 (1983).
[46] D. C. Papageorgopoulos, B. Berenbak, M. Verwoest, B. Riedmüller, S. Stolte, and A. W. Kleyn, Chem. Phys. Lett. **305**, 401 (1999).
[47] J. Harris, in *Dynamics of Gas–Surface Interactions*, edited by C. T. Rettner and M. N. R. Ashfold (Royal Society of Chemistry, Cambridge, England, 1991), pp. 1–46.
[48] B. Hellsing, M. Persson, and B. I. Lundqvist, Surf. Sci. **126**, 147 (1983).
[49] H. F. Winters, H. Coufal, C. T. Rettner, and D. S. Bethune, Phys. Rev. B **41**, 6240 (1990).
[50] J. Kimman, C. T. Rettner, D. J. Auerbach, J. A. Barker, and J. C. Tully, Phys. Rev. Lett. **57**, 2053 (1986).
[51] T. F. Hanisco, C. Yan, and A. C. Kummel, J. Chem. Phys. **97**, 1484 (1992).
[52] A. C. Luntz, A. W. Kleyn, and D. J. Auerbach, Phys. Rev. B **25**, 4273 (1982).
[53] C. T. Rettner, J. Kimman, and D. J. Auerbach, J. Chem. Phys. **94**, 734 (1991).